Cascade of Shocks in Inertial Liquid-Liquid Dewetting

X. Noblin,[1,2,*] A. Buguin,[1] and F. Brochard-Wyart[1]

[1]*Institut Curie, CNRS UMR 168, 26 rue d'Ulm, Paris, 75248 France*

[2]*OEB and DEAS, Harvard University, Cambridge, Massachusetts 01238, USA*

(Received 27 October 2005; published 19 April 2006)

We study the inertial dewetting of water films (A) (thickness e) deposited on highly hydrophobic liquid substrates (B). On these ideal surfaces, thin films can be made which dewet at large velocities obeying under those conditions the Culick law for the bursting of soap films. The rim collecting the water film can become coupled to the surface waves characterized by a surface tension $\tilde{\gamma}_B$ upstream of the rim (coated substrate) and $\gamma = \gamma_B$ downstream, where the water film has dried. Upon decreasing the thickness, we observe a sequence of two hydraulic shocks during the dewetting inducing gravity waves behind the rim, and capillary waves ahead.

DOI: 10.1103/PhysRevLett.96.156101 PACS numbers: 68.05.−n, 47.35.−i, 68.08.Bc

Introduction.—A liquid film standing on a nonwettable surface tends to dewet, exhibiting dry patches. This process plays an important role in many applications of chemical engineering (e.g., spontaneous drying, adhesion on wet substrates,...). Thick horizontal films are stabilized by their own weight. They become unstable below a certain thickness e_c. Dry holes nucleate around defects, and grow with increasing radius $R(t)$ surrounded by a liquid rim collecting the liquid. Various regimes [1–4] are found for $R(t)$ depending on the viscosity of the liquid: from polymer melts down to water, which can give inertial features.

Here we discuss the ultrafast dewetting of a water film deposited on a (nonmiscible) liquid bath (Fig. 1), as opposed to previous studies on the dewetting of water above a hydrophobic solid [4]. The liquid support is favorable because it is free of defect—there is no hysteresis at the contact line—and we can deposit much thinner water films. Our main motivation for using a liquid substrate is the possibility of shock waves induced by the fast dewetting. For any object (duck, boat, rim,...) moving at velocity V on the surface of a calm liquid, complicated wave patterns (e.g., wakes) are generated when the velocity becomes larger than the minimum phase speed, e.g., $C_{\min} = \sqrt{4g\gamma/\rho}$, where γ = surface tension, ρ = liquid density, and g is the acceleration of gravity. In our case, waves can be emitted from the front of the rim, where the liquid bath is coated by the water film, and also from the back of the rim, where the substrate is "dry." These new possibilities of shock waves propagating towards the nucleation center of the dewetting film and outwards are discussed here. On the other hand, the liquid support brings in some complications: the effective mass of the water rim is increased by a contribution due to the flows in the liquid bath.

A rim, of width L, crops all the water from the central region (radius R) (Fig. 1). For our cases of thin films ($e \ll e_c$), $L \ll R$ and the two velocities V^* at the front (point α), V at the rear (point β) have close values [$V^* = (1 + \frac{L}{2R})V \sim V = dR/dt$]. Our main aim in the present note is to study the emission of waves ahead of point α and behind point β. At low V there are no waves. When V is larger than a first threshold $C_{\min\beta}$ we see the onset of β waves. When V becomes larger than a higher threshold $C_{\min\alpha}$ we observe both α and β waves. In the following section, we describe our methods of observations and the results for $V(e)$. Then we give a theoretical prediction for $C_{\min\alpha}$ and $C_{\min\beta}$ and present our results on the waves observed. We also incorporate another delicate effect: the height of the central zone changes (for hydrostatic reasons) after elimination of the water film.

Materials and Methods.—The liquid A is ultra pure water or a dye solution (new methylene blue). We have checked that this solute does not affect the surface properties of the water for the concentrations used. The liquid B is Perfluorodecalin (PFD, $C_{10}F_{18}$, $\rho_B = 1910\ \mathrm{kg\,m^{-3}}$): immiscible with water and incompatible with the dye.

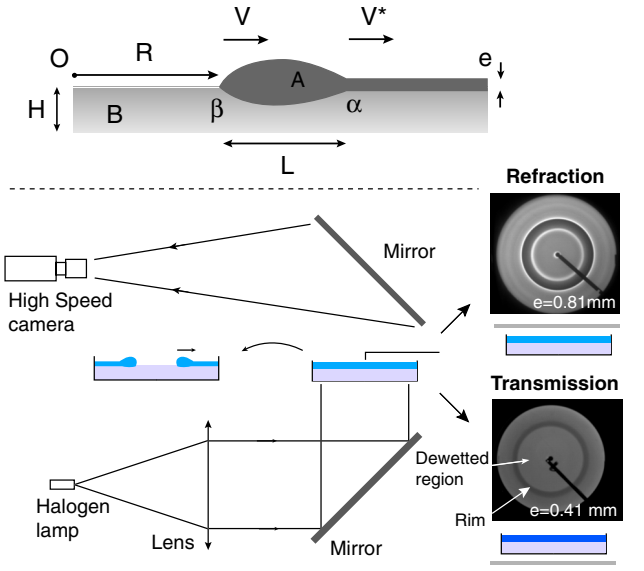

FIG. 1 (color online). Top: Dewetting of a water film A floating on a hydrophobic liquid bath B. Bottom: Experimental setup. By refraction, the diffuser is above the Petri dish, by absorption it is below (dye solution).

The spreading coefficient of water on PFD is $S = \gamma_B - (\gamma_A + \gamma_{AB})$, where $S = -109$ mN m^{-1}. The critical thickness e_c [$\frac{1}{2}\tilde{\rho} g e_c^2 = -S$ where $\tilde{\rho} = \rho_A(1 - \rho_A/\rho_B)$] is $e_c = 6.8$ mm. A glass Petri dish (diameter 200 mm) is filled with $H = 10$ mm of PFD, and covered by a thick film of water ($e > e_c$). The water spreads across the entire surface and forms a wetting meniscus on the glass walls that anchors the film. We then puncture water through a syringe needle placed in the meniscus up to the desired film thickness below e_c. The nucleation of a hole is induced by a Teflon tip linked to a motorized translation stage. The tip touches the A-air surface and then reaches the A-B interface. At this height, a PFD meniscus climbs on the hydrophobic tip thus creating a hole in the water film. The dewetting is observed only if the initial hole radius is larger than a critical radius R_c [5]. In our experiments, the tip diameter is large enough to always induce the dewetting in our thicknesses range (200 to 2500 μm).

During the dewetting, water is collected in a growing torus-shaped rim. The dewetting stops when the rim reaches the edge of the Petri dish, resulting in a final state where a bare substrate and a water ring (thickness e_c) at the edge coexist. After dewetting we cover the substrate with water and another experiment can take place. Two methods have been used to measure the film thickness and to visualize the dewetting process Fig. 1.

(i) Light absorption.—The dye solution is used, presenting a maximum absorption around the He-Ne laser wavelength (633 nm). From intensity measurement we derive the initial film thickness with high accuracy (Beer-Lambert law). Parallel illumination (halogen source filtered around 633 nm) goes vertically from below through a diffuser then the Petri dish. Observation is made from above with a fast camera (250 images/s). The dewetted surface appears bright, allowing automatic measurements of the dewetting radius $R(t)$ (see bottom image in Fig. 1).

(ii) Refraction.—The position of a tilted laser beam after reflection at the pure water-air interface is measured, providing a direct determination of the interface height. The reflection on the water-PFD interface is negligible and its position is determined before sucking water by contacting it with the Teflon tip, giving the thickness e. The illumination is the same, with no filter, but the diffuser is now placed at a fixed distance ($D \sim 2$ cm) above the water-air interface and acts as a screen. Light rays are refracted by the PFD-air and water-air interfaces which act as local converging or diverging lenses depending on the local curvature. The bright (dark) regions correspond to convex (concave) surfaces, the rim is characterized by the brightest annulus. For small deformations, with a surface profile $h(r)$, refractive index n (almost the same for water and PFD), the light intensity on the screen is given by $I = I_0(1 + (n-1)D\frac{\partial^2 h}{\partial r^2})$.

Dewetting velocity.—During dewetting we measure the radius of the hole as a function of time: $R(t)$ using both methods. We find that R is linear in time. We report in Fig. 2 the slopes dR/dt versus film thickness e ranging from 250 to 2500 μm. As for solid substrate [4], we observe that the dewetting velocity increases when e decreases. With both methods, the experimental points collapse on a single master curve (the dye has no noticeable influence on the dynamics). One image using the absorption method is shown in Fig. 1 (bottom); note that the rim is clearly visible in dark. On the same figure (top), an image obtained with the refraction method is shown; the back of the brightest annulus gives the value of $R(t)$. At the end of the dewetting, when the rim reaches the edges of the Petri dish, we observe several oscillations of the radius around its final value R_{eq} which are the clear signature of an inertial process [6]. In the inertial regime (Reynolds number $R_e = \rho e V/\eta_A$, η_A = water viscosity, $R_e \sim 200$ in our experiments), the law for V is derived from the Culick's idea (V = constant) on the rupture of soap films. Writing that the time derivative of the rim momentum is equal to the driving force [per unit length of the rim, for $R > e_c$, one have $d(MV)/dt = Vd(\rho_A e R)/dt$], this gives [7,8]:

$$\rho_A e V^2 = \tilde{\gamma_B} - \gamma_B = |S|(1 - e^2/e_c^2) \qquad (1)$$

where $\tilde{\gamma}_B$ (γ_B) is the surface tension of the coated (bare) substrate. $\tilde{\gamma}_B = \gamma_A + \gamma_{AB} - \frac{1}{2}\rho g e^2$.

In fact, the balance of inertial and driving forces [Eq. (1)] is more difficult on a liquid substrate for two reasons: (1) the immersed part of the rim displaces locally liquid B (ventral backflows) and (2) its height varies during the dewetting of the film. For point (2) we expect two limit regimes: (i) a ''frozen'' regime described by Eq. (1) at high velocities, where the B bath cannot adjust immediately (the moving mass is $M = K\rho_A e R$ with $K = 1$). (ii) A ''quasistatic'' regime at low velocity, where the height H increases ($\Delta H = \rho_A/\rho_B e$) to equilibrate the hydrostatic pressure. The complex flows induced in the substrate lead to an increased momentum that can be roughly esti-

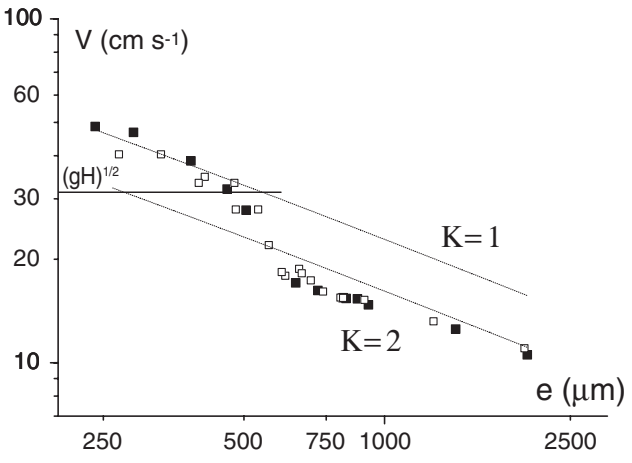

FIG. 2. Dewetting velocity as a function of thickness e. □: absorption, ■: refraction methods. The dashed lines represent Eq. (2) for $K = 1$ and $K = 2$, with a dynamical spreading parameter $S_d = S/2$. Horizontal line: speed of gravity waves in shallow water (depth $H = 10$ mm).

mated by assuming an effective mass of the rim given by $M = \rho_A eR + \rho_B(\rho_A/\rho_B)eR = K\rho_A eR$, with $K = 2$.

The experimental data for $V(e)$ show clearly two regimes. In the frozen regimes, our data for $V(e)$ fit Eq. (1) with $S_d = S/2$. We attribute this value of S_d to two contributions: (i) the added mass related to the fast ventral backflows, of order the mass of the rim, and (ii) energy losses by viscous dissipation in the boundary layer, scaling like $f_V \sim \rho_B V^2\sqrt{\frac{\eta_B l}{\rho V}} \sim 10$–$30$ mN/m [8] and waves emission (discussed later) which are both less important. We interpret the discontinuity of $V(e)$ separating the frozen and the quasistatic regime by the second effect of leveling of B liquid in the hole. The relaxation time τ of B to adjust its equilibrium thickness is given by the speed of gravity waves on shallow water $R/\tau = V = \sqrt{gH}$. Thus the crossover between the two regimes is expected for $V(e) = \sqrt{gH}$ (~ 31 cm s^{-1} for $H = 10$ mm). For $V < \sqrt{gH}$, the speed reduces until it reaches the regime with $K \sim 2$.

The Culick law on a liquid substrate, including all backflows, can be written as

$$V(e) = \sqrt{\frac{|S|(1 - e^2/e_c^2)}{2K\rho_A e}} \qquad (2)$$

with $K = 1$ for the frozen regime and $K = 2$ for the quasistatic regime [$V(e) < \sqrt{gH}$]. The factor 2 at the denominator represent the ventral backflows and dissipative effects present at all velocities.

Shock waves.—Rayleigh and Lamb have discussed the wave pattern obtained ahead and behind a perturbation moving faster than the surface waves [9]. Following their discussion, we detail now how the waves dispersion equation determines the shocks characteristics.

The phase and group velocities for capillary-gravity waves of wave vector q ($q = 2\pi/\lambda$, λ is the wavelength) on a liquid with surface tension γ, density ρ_B, and depth H (large compared to $\lambda/(2\pi)$) are [9]

$$c_\varphi = \sqrt{\frac{g}{q} + \frac{\gamma q}{\rho_B}}, \qquad c_g = \frac{g + 3\gamma q^2/\rho_B}{2\sqrt{gq + \gamma q^3/\rho_B}}. \qquad (3)$$

The phase velocity presents a minimum for $q = \kappa = \sqrt{\rho_B g/\gamma}$, equal to: $c_{\min} = (\frac{4g\gamma}{\rho})^{1/4}$.

For $q < \kappa$, $c_\varphi > c_g$ and for $q > \kappa$, $c_\varphi < c_g$.

For our system, (i) ahead of the rim, $\gamma = \widetilde{\gamma_B}$; (ii) behind the rim, $\gamma = \gamma_B$. This gives two sets of group and phase velocities (Fig. 3).

Energy is radiated out of the rim and wave fronts spread out at the group velocity. Hence, to observe waves ahead of the rim, one needs $c_g > c_\varphi$, which implies $q > \kappa$ (capillary waves). Conversely, to observe a shock behind the rim, the wave front has to be slower than the rim: $c_g < c_\varphi$, leading to $q < \kappa$ (gravity waves). The phase velocity of the shock waves equals the perturbation speed. The condition for a shock ahead of the rim is $V^* > C_{\min\alpha}$ (where V^* is the rim front speed). For a shock behind the rim we have $V > C_{\min\beta}$, (V is the dewetting velocity). For a thin film, $V \approx V^*$, but when e becomes comparable to e_c, V and V^* differ slightly (see Fig. 3). Hence, depending on velocities V and V^*, one can have no shock, a shock behind the rim or two shocks, one behind and one ahead of the rim. The graphs (Fig. 3) of the phase velocity for bare PFD and PFD covered by a thin water film versus wave vector are used to predict the cascade of shocks: For $V < C_{\min\beta} = 13.8$ cm s^{-1} we expect no shock; for $V > C_{\min\beta}$ and $V^* < C_{\min\alpha} = 22.6$ cm s^{-1} we expect one shock behind the rim and for $V^* > C_{\min\alpha}$, we expect two shocks, one behind and one ahead of the rim. The characteristic wave vector (q) for each shock can be read on the horizontal axis.

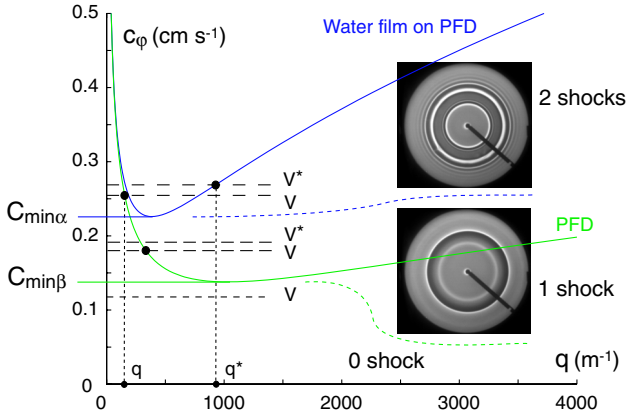

FIG. 3 (color online). Conditions of shocks behind (PFD) and ahead (water film on PFD) of the rim (increasing and decreasing branch, respectively, of the phase velocity curve).

Ahead of the rim.—We present in Fig. 4 dewetting images (refraction method) of waves patterns, ahead of the rim, for different thicknesses e. For $e \geq 0.8$ mm, there is no shock because $V^* < C_{\min\alpha}$. For $e < 0.7$ mm there is a shock, with a wavelength that decreases with the thickness. In Fig. 4, we report front velocity (V^*) as a function of the observed wavelength λ. These results are in good agreement with the dispersion equation [Eq. (3), solid line] except for small wavelengths where our description is no longer valid (we assume $qe \ll 1$). For $e \sim 0.7$ mm we observe waves moving out of the rim that are not stationary in the rim's reference frame (parasitic waves). In fact when the Teflon tip touches the water-PFD interface, waves of different wavelengths are emitted, traveling with different velocities. The shock is the amplification of the wavelength

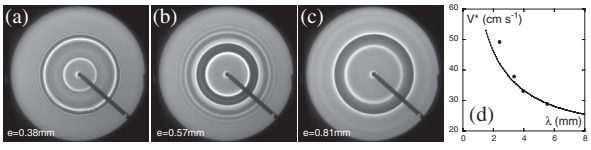

FIG. 4. Shocks ahead of the rim. (a) $e = 0.38$ mm; (b) $e = 0.57$ mm, *shock*: $V^* > C_{\min\alpha}$; (c) $e = 0.81$ mm (no shock, $V^* < C_{\min\alpha}$). Image diameter: 185 mm. (d) Front velocity (V^*) as a function of the observed wavelength λ.

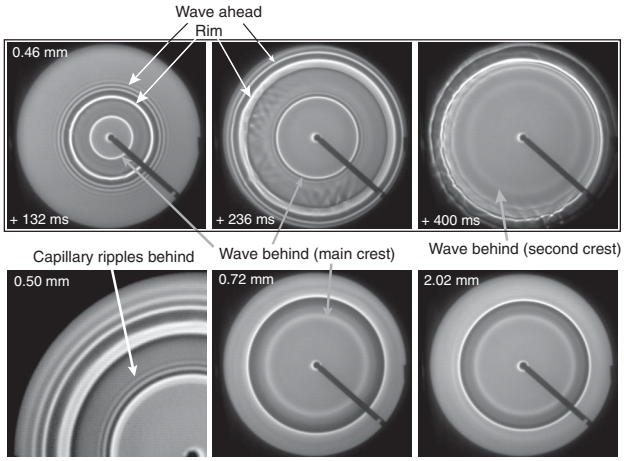

FIG. 5. Top: $e = 0.46$ mm (2 shocks, $V^* > C_{\min\alpha}$, $V > C_{\min\beta}$), 3 successive images: one can see the main crest behind the rim, and later a second crest. Bottom: Left: $e = 0.5$ mm (2 shocks), capillary ripples ahead of the shock behind the rim (only the upper left part of the global image is shown). Center: $e = 0.72$ (1 shock, behind, $V^* < C_{\min\alpha}$, $V > C_{\min\beta}$): the main crest behind travel slower than the rim. Right: $e =$ 2.02 mm (No shock, $V^* < C_{\min\alpha}$, $V < C_{\min\beta}$). Image diameter: 185 mm.

that propagates at the front velocity V^*. For thicknesses in the range 0.6–0.8 mm, the Petri dish is too small: the system does not have enough time to select and amplify the characteristic wavelength. For $e < 0.6$ mm, the dewetting is faster, and such selection is observed (Fig. 4). For thicknesses $e > 0.8$ mm, the dewetting is so slow that the initial waves have already disappeared while the rim is still far from the border of the vessel.

Behind the rim.—We present in Fig. 5 waves patterns for different thicknesses e. We clearly observe a deformation behind the rim, which propagates inward in the rim reference frame for dewetting velocities higher than 15 $\mathrm{cm\,s^{-1}}$. We checked that the higher the dewetting velocity, the larger the difference between the rim and the wave behind (see Fig. 5). This is in good agreement with the theory of gravity waves: the group velocity declines progressively to half the phase velocity at high speed. For lower dewetting velocities, we do not observe any deformation traveling slower than the rim (the main crest remains just behind it). This is in good agreement with the minimum wave velocity on PFD, $C_{\min\beta} = 13.8\ \mathrm{cm\,s^{-1}}$. The number of wavelengths n we can observe indeed grows with time, illustrating the nonsteady feature of the phenomena. n is given by $n = (c_\phi - c_g)t/\lambda$. The maximum value for n is obtained when the rim reaches the border of the Petri dish (radius R), after a time $t = R/c_\phi$: $n_m(\lambda) = (1 - c_g/c_\phi)R/\lambda$. A global maximum is reached for $n_m(\lambda)$ at $\lambda = 11.8$ mm, $n_m = 2.3$. In Fig. 5, the third image in the top row shows the second crest of the wave pattern. For smaller and larger wavelengths (corresponding to smaller and larger dewetting speeds), the number of observable wavelengths decreases. A vessel at least 1 m in size would be necessary to measure wavelength as a function of dewetting speed. In Fig. 5, for $e = 0.5$ mm, secondary waves behind the rim can be seen; these are capillary waves (small wavelengths) emitted by the main crest.

Conclusion.—We have studied the fast dewetting of a water film from an immiscible liquid substrate. Under a critical thickness e_c, dewetting occurs by nucleation and growth of a hole in the film. The dewetting velocity (up to $0.7\ \mathrm{m \cdot s^{-1}}$) remains constant during the entire process, as predicted by the inertial theory. Two major effects slow down the dewetting: the added mass of the moving rim at all velocities, and the height variation in the quasistatic regime at low velocity (a frozen regime is observed at high velocity). Viscous losses and wave resistance [10] have a smaller contribution than the flows induced in the substrate. Therefore the dewetting is slower but still inertial-like (constant speed and $V \propto e^{-1/2}$). We observe a cascade of two shocks. Ahead of the rim, we observed "α" capillary waves and measure their wavelength as a function of the rim front speed V^*. These waves are easy to characterize due to their short wavelength. Behind the rim, "β" gravity waves travel with centimetric wavelengths, and a maximum of two ripples appear, due to the finite size of the Petri dish. Nevertheless we were able to observe a characteristic deformation moving outwards but slower than the rim, as predicted by theory, due to the lower value of the group's velocity. At high speed, the shock wave behind the rim induces capillary ripples in front of itself, leading to an unexpected third shock.

We thank P. G. de Gennes, E. Rojas, J. Westbrook, and F. Rockwell for their critical reading of the manuscript.

*Electronic address: xnoblin@oeb.harvard.edu

[1] P. G. de Gennes, F. Brochard-Wyart, and D. Quere, *Capillarity and Wetting Phenomena: Drops, Bubbles, Pearls, Waves* (Springer, New York, 2003).
[2] C. Redon, F. Brochard-Wyart, and F. Rondelez, Phys. Rev. Lett. **66**, 715 (1991).
[3] G. Debregeas, P. Martin, and F. Brochard-Wyart, Phys. Rev. Lett. **75**, 3886 (1995).
[4] A. Buguin, L. Vovelle, and F. Brochard-Wyart, Phys. Rev. Lett. **83**, 1183 (1999).
[5] C. Andrieu, C. Sykes, and F. Brochard-Wyart, J. Adhes. **58**, 15 (1996).
[6] X. Noblin, A. Buguin, and F. Brochard-Wyart, Eur. Phys. J. E **14**, 395 (2004).
[7] F. E. C. Culick, J. Appl. Phys. **31**, 1128 (1960).
[8] F. Brochard-Wyart, P. Martin, and C. Redon, Langmuir **9**, 3682 (1993).
[9] H. Lamb, *Hydrodynamics* (Cambridge University Press, Cambridge, 1993), 6th ed.
[10] The wave resistance acting on the rim is: $f_i \sim \gamma_i a_i^2 (k_i^2 + \kappa_i^2)$, where κ_i^{-1} is the capillary length, k_i is the wavevector, γ_i is the surface tension, and a_i is the amplitude ahead and behind the rim. Looking at image gray level, we can measure a_i, leading to $f_i \sim 1\ \mathrm{mN/m} \ll |S|$.